Proceedings of the Institution of Mechanical Engineers, Part A: Journal of Power and Energy,
Volume 233, Issue 6, September 2019, pp. 786-802
DOI:10.1177/0957650918812510

Performance-Based Fault Diagnosis of a Gas Turbine Engine Using an integrated SVM and ANN method

Amare Desalegn Fentaye[a], Syed Ihtsham Ul-Haq Gilani[a], Aklilu Tesfamichael Baheta[a]*, Yi-Guang Li[†]

[a]Mechanical Engineering Department, Universiti Teknologi PETRONAS, 32610 Tronoh, Malaysia
[†]School of Aerospace, Transport and Manufacturing, Cranfield University, Cranfield, Bedford MK43 0AL, UK
*Corresponding author. E-mail address: aklilu.baheta@utp.edu.my

ABSTRACT

An effective and reliable gas path diagnostic method that could be used to detect, isolate, and identify gas turbine (GT) degradations is crucial in a GT condition-based maintenance. In this paper, we proposed a new combined technique of artificial neural network (ANN) and support vector machine (SVM) for a two-shaft industrial gas turbine engine gas path diagnostics. To this end, an autoassociative neural network (AANN) is used as a preprocessor to minimize noise and generate necessary features, a nested support vector machine (SVM) to classify gas path faults, and a multilayer perceptron (MLP) to assess the magnitude of the faults. The necessary data to train and test the method is obtained from a performance model of the case engine under steady-state operating conditions. The test results indicate that the proposed method can diagnose both single and multiple component faults successfully and shows a clear advantage over some other methods in terms of multiple fault diagnosis. Moreover, 5 - 8 sets of measurements have been used to assess the prediction accuracy, and only a 2.3% difference was observed. This result indicates that the proposed method can be used for multiple fault diagnosis of GTs with limited measurements.

Keywords: sensor; gas turbine; artificial neural network; support vector machine; gas path diagnostics.

1. INTRODUCTION

GT performance deterioration highly influences its reliability, availability and lifetime. Thus, there is a need to obtain an accurate and reliable gas path diagnostic system to support a reliable, efficient, safe, and cost-effective operation. The health status of gas turbine gas path components is represented by health parameters (flow capacity and isentropic efficiency indices) that may change due to engine deterioration. They can be assessed based on the deviations of a set of gas path measurements (such as pressure, temperature, fuel flow rate, and shaft speed deltas) called fault signatures.

Nomenclature and Abbreviations

ANN	Artificial neural network
AANN	Auto-associative neural network
C	Compressor
CF	Compressor fouling
DCF	Double component fault
F	Fault
FNR	False negative rate
FPR	False positive rate
GG	Gas generator
GGTE	Gas generator turbine erosion
GPA	Gas path analysis
GSP	Gas turbine simulation program
HP	Hyperplane

KL	Kalman filter
MCF	Multiple component fault
ML	Machine learning
MLP	Multilayer perceptron
MSE	Mean square error
NCFD	Number of correct fault detections
NCNFD	Number of correct no-fault detections
NF	No-fault
NFC	Number of fault cases
NIFD	Number of incorrect fault detections
NLR	National aerospace laboratory
NNFC	Number of no-fault cases
NNFD	Number of no-fault detections
OvA	One-vs-all
OvO	One-vs-one
PC	Principal component
PT	Power turbine
PTE	Power turbine erosion
SCF	Single component fault
SF	Sensor fault
SVM	Support vector machine
TCF	Triple component fault

TNR	Total negative rate
TPR	Total positive rate
Γ	Flow capacity
η	Efficiency
μ	Mean
σ	Standard deviation
ρ	Correlation coefficient
Δ	Delta

The accuracy of gas path diagnostics is affected by measurement uncertainties. In order to attain a more reliable diagnostic results, either the measurement uncertainties should be dealt with properly, prior to the gas path diagnosis, or the gas path diagnostic method should be capable of tolerating the uncertainties. Moreover, the number of instruments available may be limited due to reasons such as sensor installation and maintenance costs. This may lead to a poor observability of engine health.

Studies in the past introduced several gas path diagnostic techniques for both industrial and aircraft applications (1). The traditional techniques such as gas path analysis (GPA) and Kalman filter (KF) have limitations in terms of undertaking noise and bias effects, possibility of false alarms due to the smearing effects, the number of sensors required to provide an accurate diagnostic solution, ability to efficiently under take the nonlinearity nature of the engine behavior, and solution convergence problem for large fault values (2-4). Recent studies on gas path diagnostics have thus made more efforts on applications of artificial intelligence methods such as ANNs, for this task. For instance, a multiple sensor fault (SF) diagnosis method using a bank of AANNs was introduced by Zedda and Singh (5) for a low-bypass-ratio

turbofan engine. Ogaji et al. (6) also investigated the potential of nested ANNs to diagnose single and double SFs in a two-shaft GT engine. A similar technique was used by Joly et al. (7) for single and double component fault diagnosis in a two-shaft aircraft engine. These two studies considered both qualitative and quantitative diagnosis and were able to diagnose all the considered fault scenarios with a reasonably good accuracy. Two years later, Xiradakis and Li (8) applied bank of multilayer perceptron (MLP) nets for SF detection, quantification, and accommodation in a two-shaft industrial gas turbine engine. On another study, the use of an ANN for single and multiple component fault (MCF) classification and identification of a turbofan engine was investigated by Ogaji et al. (9) based on a transient data.

Recently, nested ANNs (10) and Associative NN (11) were used for single and double sensor/component fault diagnosis. Although the results obtained were encouraging, they were restricted to qualitative diagnosis. More recently, a quantitative SF diagnosis was made by Courdier and Li (12) using nested ANNs. Dynamic NN identifiers were also developed by Amozegar and Khorasani (13) for GT diagnostics, which indicated that the performance of the ensemble method was significantly better than the individual nets. Nowadays, SVM for gas path diagnosis is getting attention (14, 15). It was utilized in machine condition monitoring applications (16) and provided better classification results than other machine learning (ML) techniques (17).

In this paper, a new gas path diagnostic scheme is developed by integrating an AANN, an SVM, and an MLP techniques. It has been applied to a two-shaft industrial GT engine under steady-state operating conditions where single, double, and triple component fault (TCF) scenarios were considered along with measurement uncertainties. Furthermore, the impact of the number of sensors on the detection and classification performance of the proposed method has been investigated. Finally, the performance of the proposed method is compared with that of some other methods published in the literature.

2. COMBINED AANN-SVM-MLP FAULT DIAGNOSTIC SCHEME

In a practical engine diagnostics, usually, a fault diagnostic system requires three basic activities; data acquisition, data processing and decision making. Data acquisition is the process of collecting and storing the necessary engine performance data. The data processing task involves noise reduction and pattern generation, through appropriate data screening techniques. Whereas, decision making is the last and the most important part, in which algorithms are applied to detect, isolate and identify various faults. As shown in Figure 1, our proposed gas path diagnostic method consists of 11 modules. The first module (AANN based) is for data processing, the next 9 modules (SVM based) are for fault detection and isolation, and the last module (MLP based) is for fault identification. The degradation of major gas turbine gas path components, such as compressor fouling (CF), gas generator turbine erosion (GGTE), and power turbine erosion (PTE)) were considered together with measurement uncertainties.

During diagnostics, engine fault signature is fed into SVM1 to distinguish faulty (F) and no-faulty (NF) engine. If it indicates a faulty engine, the fault signature is then passed to SVM2 for the classification of single component fault (SCF) or MCF. Then SVM3, SVM4, and SVM5 are applied to classify each SCF, SVM6 to classify double component fault (DCF) and TCF, and SVM7, SVM8, and SVM9 to classify each DCFs. Table 1 presents the number and the types of fault classes considered in this analysis. Finally, a MLP network is used to quantify the isolated faults. The proposed gas turbine gas-path diagnostic algorithm is designed, demonstrated, and illustrated in the Matlab environment.

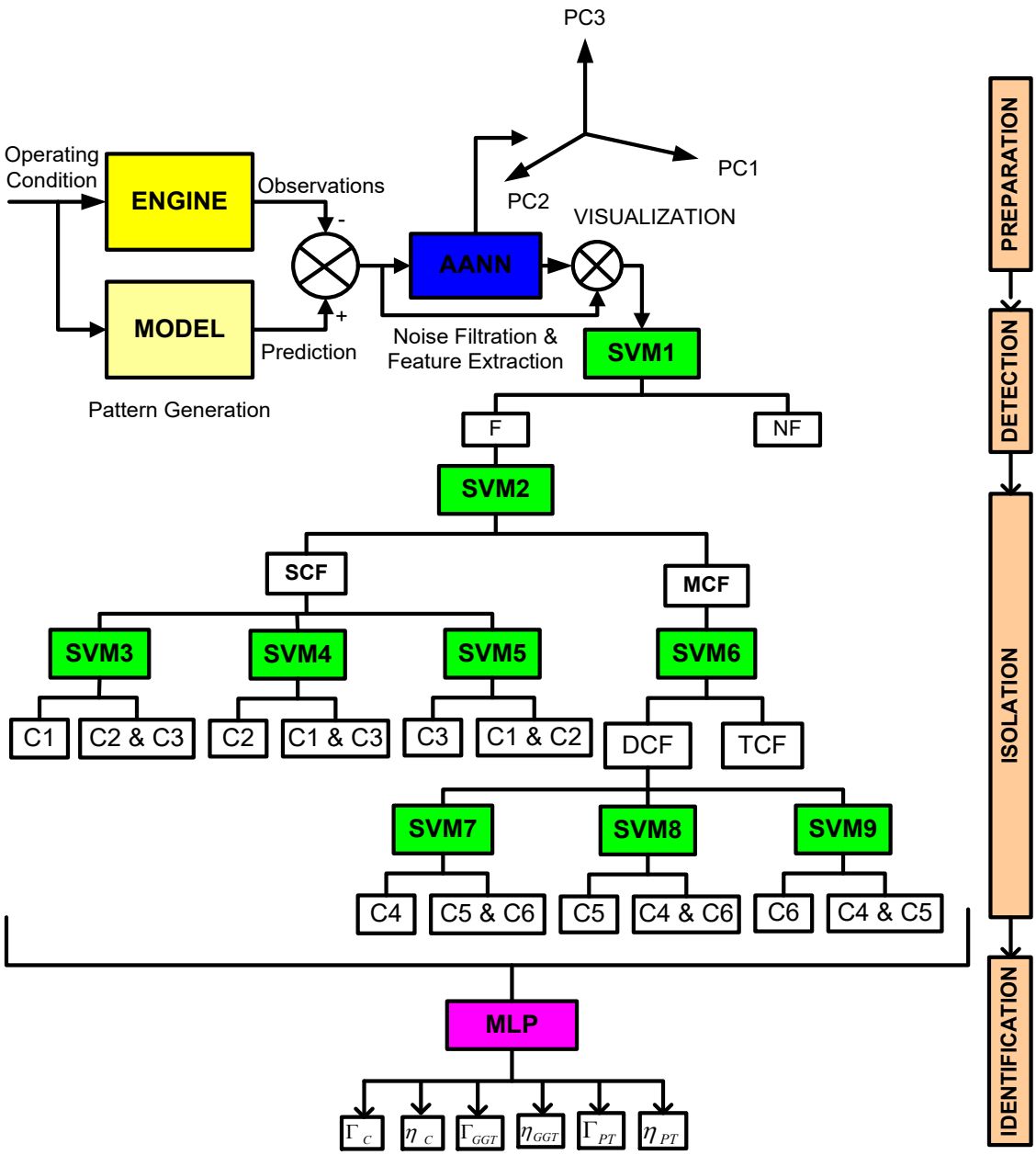

Fig. 1. Structure of the diagnostic system

Table 1: Types of fault classes considered in fault diagnostics

Case	Class type	Designation
1	No-fault	NF
2	CF	C1
3	GGTE	C2
4	PTE	C3
5	CF+ GGTE	C4
6	CF+ PTE	C5
7	GGTE + PTE	C6
8	CF+ GGTE + PTE	C7

2.1 Auto-Associative Neural Networks

2.1.1 **Structure and training**

An AANN is a computing paradigm that learns an approximation to the identity function in an unsupervised manner to give an output similar to its input (18). The general topology of a five-layer AANN, as shown in Figure 2, is composed of an input layer, a mapping layer, a bottleneck layer, a de-mapping layer, and an output layer. The bottleneck layer is located in the middle of the network, with the smallest number of neurons, where the feature vector is captured.

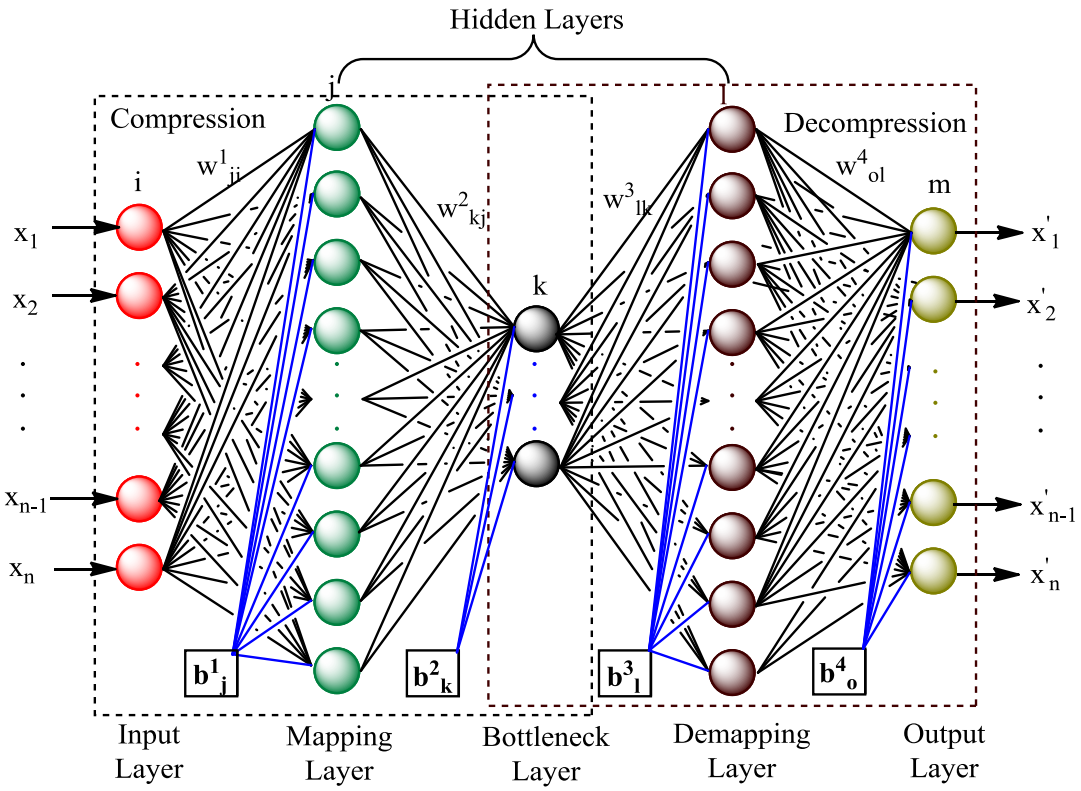

Fig. 2. General structure of AANN

When the training of the AANN, a group of training samples is fed into the input layer. The AANN will learn a way to produce reconstructed values that can be compared with the desired output. The error is then back-propagated to modify NN parameters (gradients, biases, and weights) in iterations till the training is completed. During the training, the Mean Square Error (MSE), Eq. (1), between the reconstruction and the target is minimized. Meanwhile, the generalization performance of the AANN is checked using test samples.

$$MSE = \frac{1}{N}\sum_{i=1}^{N}\left(y_p - y_t\right)^2 \tag{1}$$

where y_p is the network output, y_t is the target value, and N is the number of samples.

2.1.2 Data Denoising and Feature Extraction Using an AANN

Measurement noise is one of the main sources of inaccurate fault diagnosis. Due to the engine's harsh operating conditions, high-level of noise may be of the same order of magnitude with the low-level component faults, is more likely to occur (19). If this effect is ignored while developing a fault diagnostic system, the solution will be unrealistic. Conversely, an attempt to detect actual gas-path component faults using high-level sensor noise corrupted data may encounter a large number of false alarms or missed detections. Data processing and validation (denoising the data using an appropriate data screening technique) is thus one of the very important tasks to be accomplished prior to a fault diagnostics. This helps to minimize the influence of the measurement noise and enhance diagnostic accuracy (20). There are several conventional data filtering methods available in the open domain implemented for gas turbine engines previously such as Myriad filter, Median filter, and Kalman filter (21). An AANN is the most widely used data filtering and validation technique among the AI methods (5, 6, 18, 22, 23). Vanini et al. (11) used this technique for outliers removal and noise minimization in a two-shaft aircraft engine. It has been reported that their proposed technique has shown a noteworthy outliers removal and noise minimization capability in for most of the measurement parameters (from 33% to 92%).

The AANN structure shown in Figure 3 was used to smooth the data and extract features for visualization. The data with measurement noise were used as input and the data with true values as output to form training samples. During the forward propagation of the training process, the first portion of the network converts the input data into a feature space at the bottleneck layer and the second portion of the network reconstructs the data at the output layer. After the training, the network will have the capability to filter the measurement noise and provide the output that is close to the expected target.

The features of the data were extracted from the bottleneck layer. The most significant Principle Components (PCs) were selected and the feature vectors may be plotted in the feature space using PCs as axes. Such procedure is summarized in Figure 4.

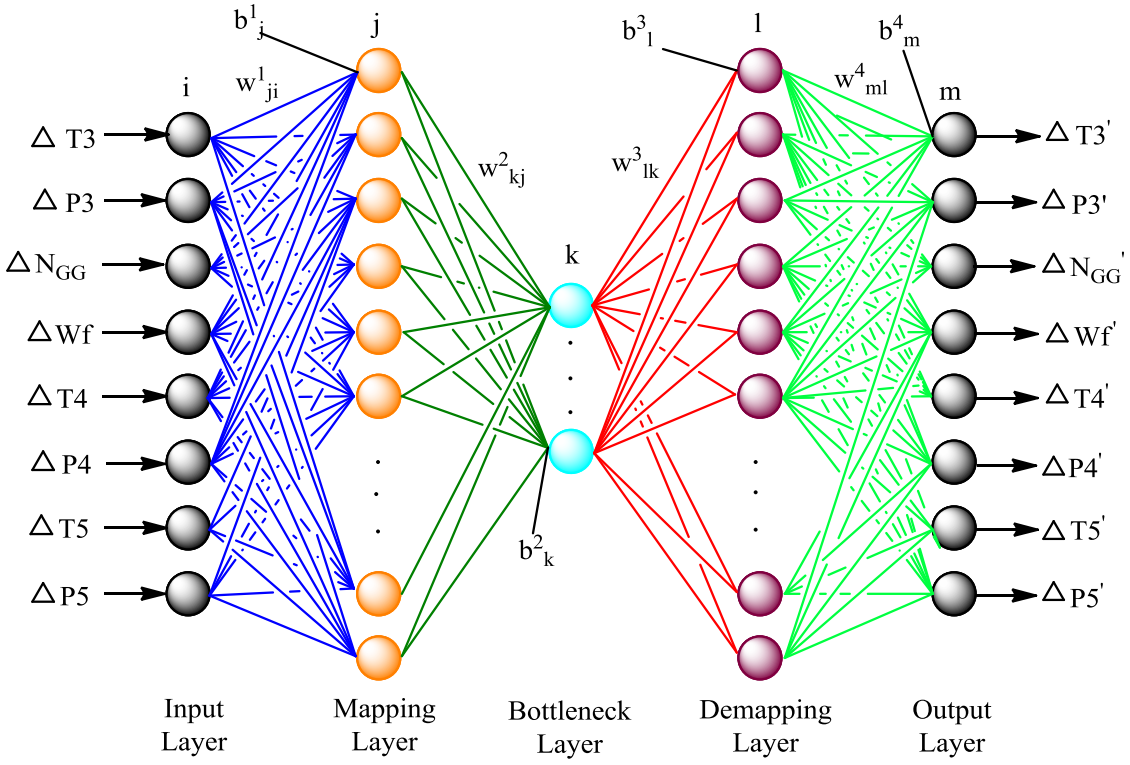

Fig. 3. AANN structure for GT noise minimization and feature extraction

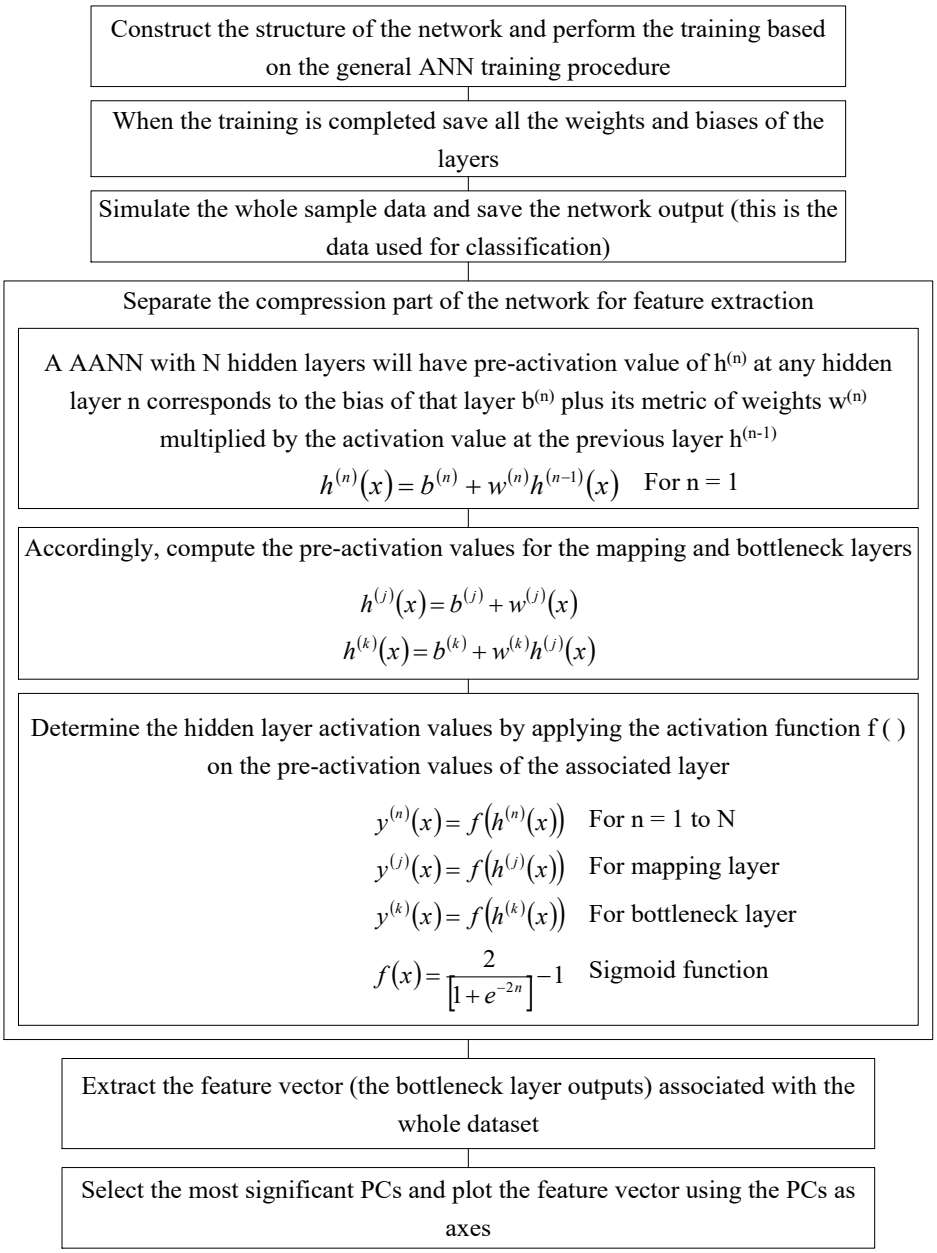

Fig. 4. AANN based data de-noising and feature extraction

2.2 Component Fault Detection and Isolation using SVM

2.2.1 SVM classification Principles

SVM is one of the most popular supervised learning algorithms (15). It is a binary classifier that separates classes into two groups at a time, based on a one-vs-all (OvA) or one-vs-one (OvO) (16) approach. The objective of training an SVM is to find the best separating hyperplane (HP). The classification effectiveness of this method could be increased by maximizing the margin between the classes.

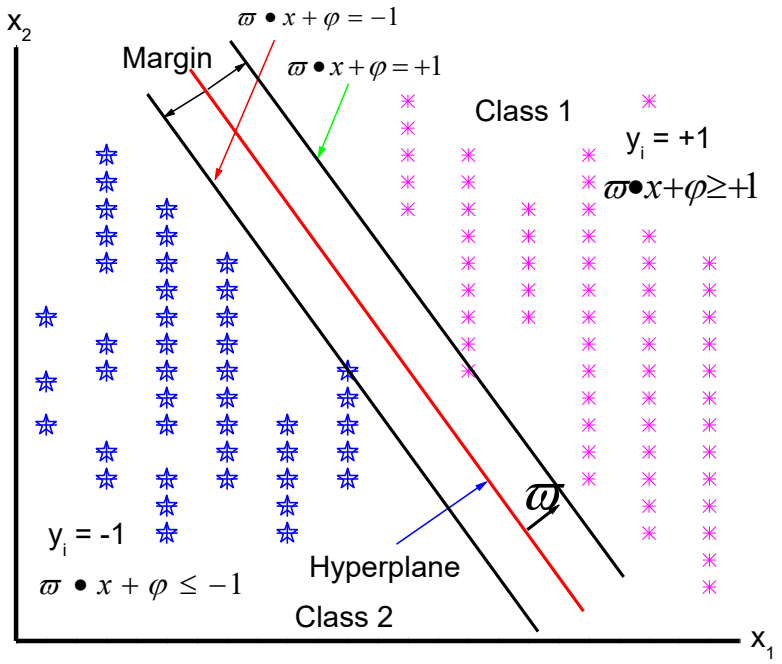

Fig. 5. Schematic illustration of SVM based classification

Assuming there are two classes C1 and C2 as shown in Figure 5 where x1 and x2 refers to the dimensions of the feature vector. The HP may be expressed by Equation (2).

$$f(x) = \varpi^T x + b \tag{2}$$

where ϖ is the weight vector that is perpendicular to the HP, x is the input feature vector, and b is the bias that represents the location of the HP in the feature space.

For a new feature x_{new}

$$\text{If } f\left(x_{new}\right)=\varpi^{T}x_{new}+b>0\Rightarrow x_{new}\in C1 \tag{3}$$

$$\text{If } f\left(x_{new}\right)=\varpi^{T}x_{new}+b<0\Rightarrow x_{new}\in C2 \tag{4}$$

$$\text{If } f\left(x_{new}\right)=\varpi^{T}x_{new}+b=0\Rightarrow x_{new} \text{ falls on the HP} \tag{5}$$

If the label y_i is +1 for C1 and -1 for C2:

$$\forall_{i=1}^{p}: y_i \bullet \left(\varpi \bullet x_i + b\right) > 0 \tag{6}$$

The perpendicular distance of a new point p from the HP can be computed as:

$$d_p = \frac{\varpi \bullet x + b}{\left\|\varpi\right\|} \tag{7}$$

For a confidential classification, *dp* should be greater than or equal to certain margin ζ

$$\frac{\varpi \bullet x + b}{\left\|\varpi\right\|} \geq \zeta \Rightarrow \varpi \bullet x + b = \zeta\left\|\varpi\right\| \tag{8}$$

By applying a proper scaling, Equation (8) becomes Equation (9).

$$\varpi \bullet x + b = \zeta\left\|\varpi\right\| = 1 \tag{9}$$

$$\text{If } \varpi \bullet x + b \geq 1 \Rightarrow x \in C1 \tag{10}$$

$$\text{If } \zeta\left\|\varpi\right\| \leq 1 \Rightarrow x \in C2 \tag{11}$$

In order to maximize the margin to separate the two classes, the distance between the closest points need to be maximized (Eq. (12)).

$$\max_{\{\varpi,\varphi\}} \frac{1}{\|\varpi\|} \text{ or } \min_{\{\varpi,\varphi\}} \frac{1}{2}\|\varpi\|^2 \text{ subject to } y_i \bullet (\varpi \bullet x_i + 1) \geq 1, \quad i = 1,2,\ldots, k \tag{12}$$

The maximization function in the form of Lagrange dual optimization function is given as:

$$\max_{0 \leq \alpha \leq R} = \sum_i \alpha_i - \frac{1}{2}\sum_j \alpha_i \alpha_j y_i y_j \left(\vec{x}_i \bullet \vec{x}_j \right) \text{ subject to } \alpha_i = 0 \text{ and } \sum_i \alpha_i y_j = 0 \tag{13}$$

where α is Lagrange Multiplier

The optimized solution may be represented by Equation (14).

$$f(x) = sign\left(\sum_{i=1} \alpha_i y_i \vec{x}_i \vec{x} + b \right) \tag{14}$$

For classes that are not linearly separable, the data points are projected into a higher dimensional space so that they become linearly separable. For this projection, Kernel functions are commonly used (15). The idea is, for a given Kernel function $K(x_i, x_j)$, the nonlinear input vector ($\vec{x}$) can be mapped into a high-dimensional space through a transformation functions ($\Psi(\vec{x})$)), as of Eq. (15).

$$\Psi : \vec{x} \rightarrow \phi(\vec{x}) \tag{15}$$

The dot product would become:

$$K(x_i, x_j) = \phi(x_i^T)\phi(x_j) \tag{16}$$

The objective function to be minimized and the nonlinear HP decision function are expressed by Eqs. 17 and 18, respectively (24).

$$\max_{0\le\alpha\le R} = \sum_i \alpha_i - \frac{1}{2}\sum_j \alpha_i \alpha_j y_i y_j K\left(\vec{x_i} \bullet \vec{x_j}\right) \tag{17}$$

$$f(x) = sign\left(\sum_{i=1} \alpha_i y_i K(\vec{x}_i \bullet x) + \vec{b}\right) \tag{18}$$

where

$$b = \frac{1}{|m|}\sum_{i\in m}\left(y_i - \sum_{j=1}^{r} \alpha_j y_j (x_i \bullet x_j), \mathrm{i} \in m \equiv (i : \alpha_i \neq 0)\right) \tag{19}$$

2.2.2 Application of SVM for GT Fault Detection and Isolation

It is understandable that selecting an appropriate classification technique is very critical for an effective engine fault detection and isolation. Previously, the classification potential of an SVM has been evaluated by implementing in different fields such as medical science (25, 26), biology (27-31) and engineering (32). The reported results indicate its powerful learning ability for classification, thereby encourage incorporating this method for gas turbines too. On the other hand, many authors also showed that the classification performance of an SVM is better than an MLP (33-35). Using nested modules for classification aiming to divide and share diagnostic tasks is highly encouraged (3). Especially, dividing the diagnostic tasks systematically and arranging the associated models hierarchically provides a more detailed information about the nature of the gas-path problems. That may increase the understanding of the engine operator during the decision making. Moreover, this helps to avoid the possibility of searching a not existing fault by activating only the necessary module(s) in the hierarchy. As a result, the overall testing computational time of the diagnostic system would be reduced. The advantage of this concept has been evaluated for ANNs (3, 7) and recently for an SVM to some extent (15). Conversely, the multiple fault

classification success rate obtained from a single MLP structure, as reported in (36), may also support the utilization of SVM in general and nested SVM modules in particular.

As stated in section 2, following the data processing step, detection and isolation are the two most important parts in engine fault diagnosis. The use of multiple SVM for a SCF classification of a GT engine was studied by Zhou et al. (15). Conversely, in the current work, a different nested SVM based classification framework was developed for single, double, and triple CFs detection and isolation. Since eight classes (as presented in Table 1) were considered, the detection and isolation problem of the engine was treated as a multi-class classification problem. These classes were split into nine binary classes according to the hierarchical framework shown in Figure 1. For example, SVM1 of this framework was dedicated to distinguish normal and abnormal operating conditions of the engine, while SVMs 3-5 to separate compressor, GGT, and PT faults, respectively. Likewise, SVMs 6-8 used to classify DCFs. In general, as shown in Figure 6, the procedure of developing an SVM based model for this purpose requires three steps: feature extraction, building the model using the training samples, and testing its performance on the test samples. Supporting a SVM by a feature extraction and noise reduction technique helps to enhance its classification performance (37). In this regard, the required features were extracted from the AANN based preprocessor, as discussed in section 2.1.2. The extracted features associated with every binary class were divided into training and test samples followed by defining their corresponding class labels. Training was then performed on the training samples until the optimized classifier model obtained. After training, unlabeled test samples were fed into the model to verify its generalization performance. The complete processes flow is given in Figure 7.

Cross-validation technique was applied to control overfitting and select the best among the potential models. There are different cross-validation techniques available for ML algorithms. Two of the most

widely used techniques are holdout cross-validation and k-fold cross-validation. The former is accomplished by dividing the sample dataset into training and test groups. Whereas, in the latter case, the sample data is divided into k number of equal sized folds and the training is done on the k-1 folds while 1 fold is left for validation. This need to be done for all possible combinations. The latter approach was applied in the current work.

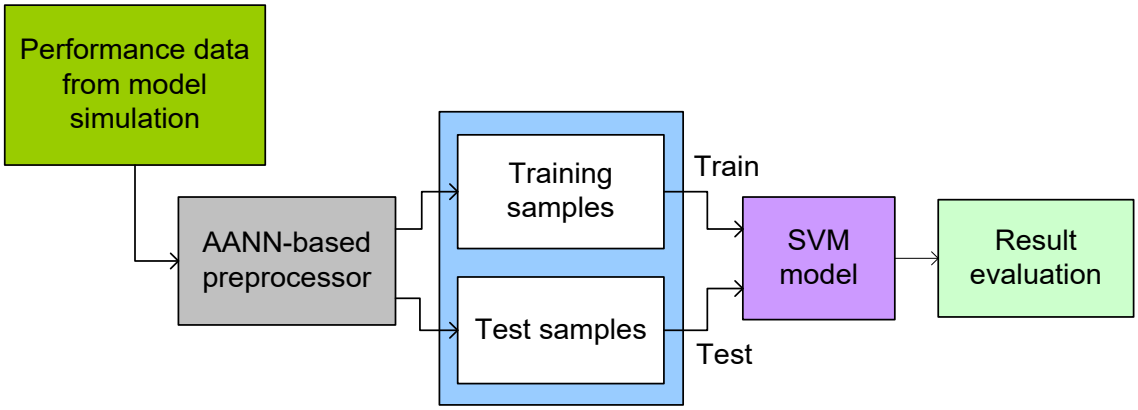

Fig. 6. SVM application for GT fault classification

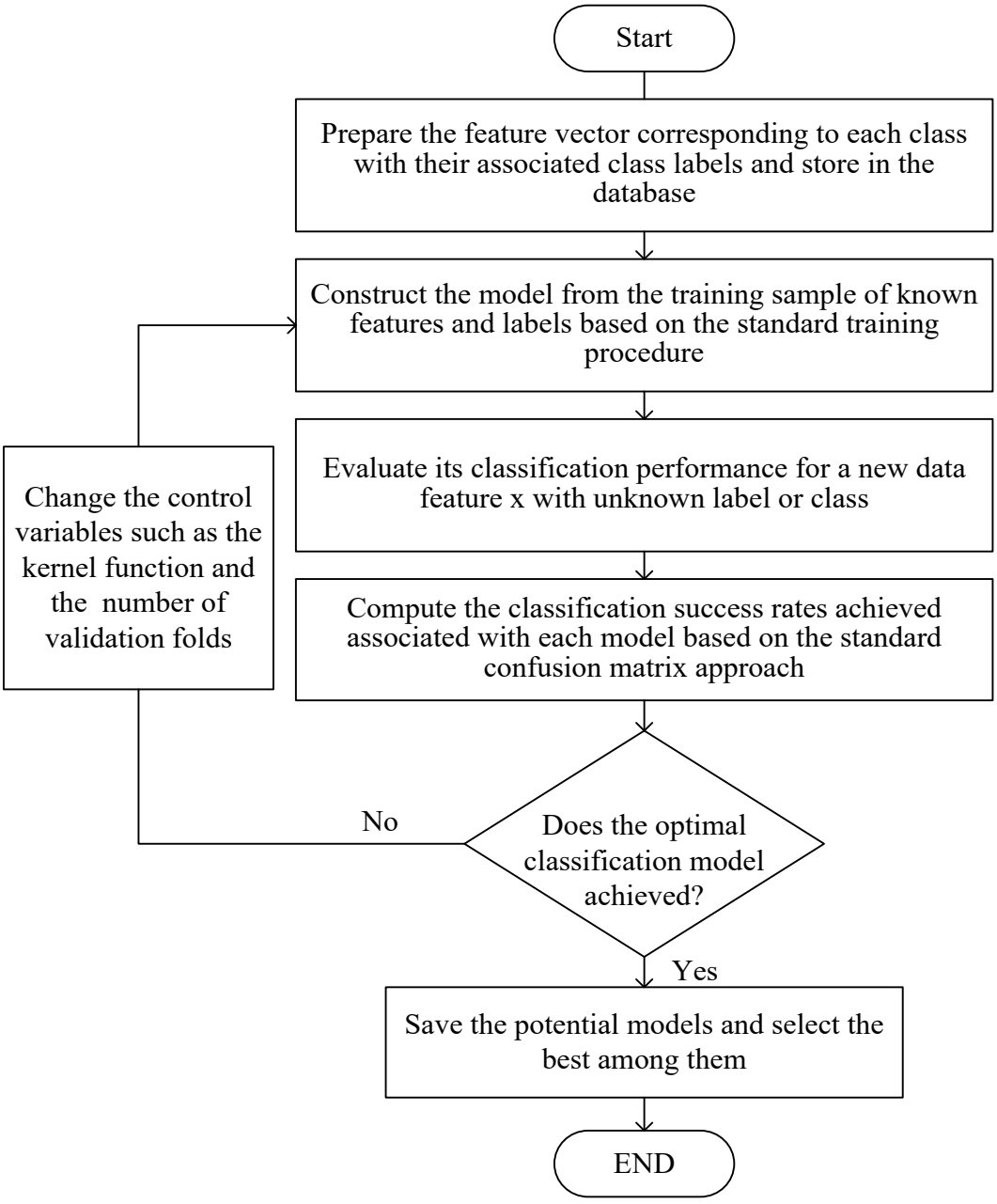

Fig. 7. SVM based GT gas path fault classification model development processes flow

2.3 Component Fault Identification Using a MLP

MLP is a feed-forward neural network type supervised learning algorithm consisting of input and output layers with one or more hidden layers in between (38). During training, the network tries to learn the relationship between input and output parameters based on training samples with the backpropagation algorithm. According to the universal approximation theorem (39), a neural network with a single hidden layer comprising of multiple nodes can approximate any input-output relationship. Hence, in this paper, a single layer MLP, as shown in Figure 8, is used to assess gas path CFs in a two-shaft GT engine. Component fault identification is a reverse process to obtain the component health parameter deviations from fault signatures. Suppose that $\Delta X_{i,j}$ and $\Delta Y_{i,j}$ represent the fault signature matrix and the fault matrix as shown in Eqs. 20 and 21, respectively, $\Delta X_{i,j}$ is input to the network while $\Delta Y_{i,j}$ is the desired output. The network was trained for fault identification using training samples derived from seven fault scenarios in an attempt to capture useful patterns from these samples and fine tune the connection weights and biases. Meanwhile, the status of estimation accuracy was evaluated in terms of MSE utilizing the training and validation data sets together.

$$\Delta X_{i,j} = \begin{bmatrix} \Delta T3_1 & \Delta P3_1 & \Delta N_{GG1} & \Delta Wf_1 & \Delta T4_1 & \Delta P4_1 & \Delta T5_1 & \Delta P5_1 \\ \Delta T3_2 & \Delta P3_2 & \Delta N_{GG2} & \Delta Wf_2 & \Delta T4_2 & \Delta P4_2 & \Delta T5_2 & \Delta P5_2 \\ \vdots & \vdots & \vdots & \vdots & \vdots & \vdots & \vdots & \vdots \\ \Delta T3_m & \Delta P3_m & \Delta N_{GGm} & \Delta Wf_2 & \Delta T4_m & \Delta P4_m & \Delta T5_m & \Delta P5_m \end{bmatrix} \quad (20)$$

$$\Delta Y_{i,j} = \begin{bmatrix} \Delta\Gamma_{C1} & \Delta\eta_{C1} & \Delta\Gamma_{GG1} & \Delta\eta_{GG1} & \Delta\Gamma_{PT1} & \Delta\eta_{PT1} \\ \Delta\Gamma_{C2} & \Delta\eta_{C2} & \Delta\Gamma_{GG1} & \Delta\eta_{GG1} & \Delta\Gamma_{PT1} & \Delta\eta_{PT1} \\ \vdots & \vdots & \vdots & \vdots & \vdots & \vdots \\ \Delta\Gamma_{Cm} & \Delta\eta_{Cm} & \Delta\Gamma_{GGm} & \Delta\eta_{GGm} & \Delta\Gamma_{PTm} & \Delta\eta_{PTm} \end{bmatrix} \quad (21)$$

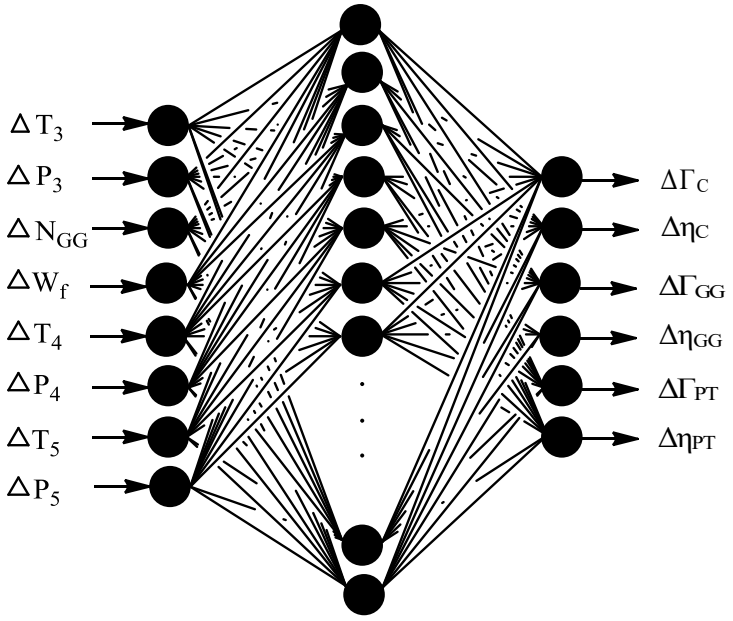

Fig. 8. MLP structure for GT fault quantification

The performance parameters' estimation errors were assessed using the two most popular statistical data analysis methods, namely standard deviation (σ) and correlation coefficient (ρ). The errors' standard deviation is used to measure how spread out the estimated values are from their mean (μ). It is useful to determine the confidence level that the approximation network produces. According to the definition of the standard distribution, 68% of the samples lies within ±1σ; 95% within ±2σ; and about 99% within ±3σ from the mean. Therefore, for ±2σ error level, which is the most frequently applied in practice, the range of the prediction accuracies of the fault identification models were computed using Eq. (22). A correlation coefficient (Eq. (23)) is another approach that evaluates the strength of the relationship between the predicted and target values. According to Provost (40), $0.9 < \rho < 1$ refers a very strong correlation, $0.8 < \rho < 0.9$ a strong correlation, and $0.7 < \rho < 0.8$ a weak correlation.

$$\hat{p} = p_{Actual} \pm 2\sigma \tag{22}$$

$$\rho = \frac{n\left(\sum pt\right) - \left(\sum p\right)\sum t}{\sqrt{\left[n\left(\sum p^2\right) - \left(\sum p\right)^2\right]\left[n\left(\sum t^2\right) - \left(\sum t\right)^2\right]}} \tag{23}$$

where p is network prediction, t is the target value, and n is the number of test samples.

3. PERFORMANCE DATA GENERATION AND PROCESSING

To train and test the introduced GT gas path diagnostic scheme, a large number of training samples from a "clean" and a deteriorated engine are required. This might be done either by intentionally ingesting faults into an operating engine and collecting measurements or by implanting fault patterns into an engine model. The former is highly expensive and not recommended (41). Consequently, a performance model of a GT engine was set up in this study to generate the required data samples.

GSP developed by NLR in the Netherlands (42) was used to generate a performance model of a GT similar to GE LM2500 (43), which is operating in an oil & gas industry at Resak PETRONAS platform in Malaysia. Figure 9 shows the schematic diagram of this model engine. The gas path parameters and their corresponding maximum measurement noise values are also given in Table 2. After completing the engine model for performance simulation, the required data was generated taking into account the ambient condition and performance deterioration effects. A gas turbine operating condition cannot be constant in most of the time due to variations in ambient condition. A common way to avoid the influence of operating conditions is to form a baseline model, compute measurement deviations, and use them as network inputs instead of measurements themselves. In order to accommodate this ambient condition variation, ambient temperature changes between -45°C to +45°C with up to 3% change in ambient pressure were considered.

Regardless of the operating condition effects, the impact of performance degradation on measurement variation provides relevant information about the condition of the engine. To avoid the effects of the ambient condition variation on the gas-path measurement deviations, all the measurement parameters are corrected against those variations based on Eq. (24). The baseline condition was set at sea-level-static (SLS) conditions for a standard day (TRef = 288.15K and PRef = 1.01325 bar).

$$X_{Measured,C} = \frac{X_{Measured}}{\theta^{\alpha} \times \delta^{\beta} \gamma^{\tau}} \tag{24}$$

where: X is the gas-path measurement parameter, θ = TMeasured/TRef is the temperature correction factor, δ = PMeasured/PRef is the pressure correction factor, α and β are temperature and pressure ratio exponents, respectively.

The value of the exponents in Eq. (24) slightly varies from engine to engine. For the case engine considered in the current work, the values of these exponents corresponding to each gas-path measurement parameter are obtained by optimizing the difference between the corrected parameter values using Eq. (24) and the reference values at the standard day condition. The obtained results from the optimization and the associated corrected parameters are presented in Table 3.

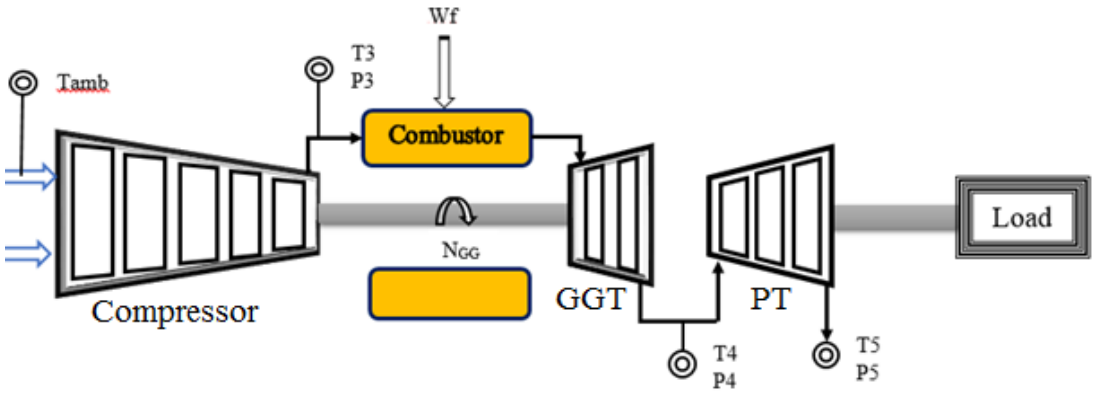

Fig. 9. Schematics of a two-shaft GT engine with gas-path measurement parameters

Table 2: Measurement parameters and maximum measurement noise

Parameter	Unit	Description	Max. Measurement Noise (±2σ)
T3	K	Compressor (C) delivery total temperature	0.4
P3	bar	Compressor delivery total pressure	0.25
N_{GG}	rpm	Gas generator (GG) relative shaft speed	0.2
Wf	Kg/s	Fuel flow rate	0.5
T4	K	GG exit/PT inlet total temperature	0.4
P4	bar	GG exit/PT inlet total pressure	0.25
T5	K	PT exit total temperature	0.4
P5	bar	PT exit total pressure	0.25

Table 3. Parameter correction exponents and equations for LM2500 engine measurements

Parameter	α	β	Corrected parameter
T3	0.94	0	$T_{3C} = \frac{T3}{\theta^{0.94}}$
P3	0	1	$P_{3C} = \frac{P3}{\delta}$
Ngg	0.5	1	$N_{GG} = \frac{N_{GG}}{\sqrt{\theta}}$
Wf	0.65	1	$W_f = \frac{W_f}{\theta^{0.63}\delta}$
T4	0.85	0	$T_{4C} = \frac{T_4}{\theta^{0.85}}$
P4	0	1	$P_{4C} = \frac{P_4}{\delta}$
T5	1	0	$T_{5C} = \frac{T_5}{\theta^{0.85}}$
P5	0	1	$P_{5C} = \frac{P_P}{\delta}$

As far as a performance deterioration is concerned, there is some inconsistency in the literature on the range of variation of the engine components flow capacity and isentropic efficiency indices and their correlation (44-46). Due to the reason that the diagnostic system should be generic in order to effectively diagnose faults that could possibly exist in the engine lifetime and due to the matter of the fact that artificial intelligence methods are not capable of performing a fault diagnosis creditably outside the training data space, a large database consisting of a wide range of fault library, taking into account the above mentioned inconsistencies, is therefore essential. This database is made of multiple measurement deviations called fault signatures, from which sets of training and test data samples are drawn. Besides, several fault diagnostic method development studies like (2, 7) also considered somewhat higher ranges than the published ranges in (44-46), aiming to increase the working space of the method. For the same reason, in the present work, a flow capacity drop of -8% to 0 and an isentropic efficiency drop of – 3.5% to 0 for compressor fouling and an increase in flow capacity ranging from 0 to +6% and an isentropic efficiency change similar to the compressor fouling were assumed. The implanted fault case patterns were then constructed within these degradation. Each component degradation was considered as two degrees of freedom problem (that is, one faulty component causes changes in its flow capacity and isentropic efficiency parameters), and it is also a common practice in the literature (7, 9, 47, 48). Accordingly, all single component faults were represented by changes in the two performance parameters, double component faults by changes in four performance parameters, and triple component faults by changes in six performance parameters expected to vary with time. While generating the fault patterns associated with the considered component fault types, the isentropic efficiency range was divided into several numbers of severity segments and each level is combined with different ratios of flow capacity drops, in the same way as (2).

The gas-path measurement deviations (ΔX) from the established baseline (XBaseline) were computed using Eq. (25). These percentage deltas refer to the fault patterns or fault indicators were then used to train and test the diagnostic system.

$$\Delta X(\%) = \frac{X_{Corrected} - X_{Baseline}}{X_{Baseline}} \times 100 \tag{25}$$

Overall, 4743 data samples (459 NF + 4284 component fault (i.e., 612 samples from each component fault scenario)) were generated and used as training and test samples. Accordingly, for SVM1 4743, for SVM2 4284, for SVM3, SVM4, SVM5, SVM7, SVM8, and SVM9 1836 each, and for SVM6 2448 learning data samples were used based on the number of classes they are dedicated to distinguishing. Likewise, of the total 4284 component fault samples, 3108 samples were used to train, validate, and test the fault estimation network, by randomly dividing it into three sub-samples (70% for training and 15% each for validation and testing). The remaining 1176 samples, were used to evaluate the accuracy.

4. RESULTS AND DISCUSSION

4.1 Data De-noising and Visualization

In order to select the right number of neurons in the hidden layers of the AANN, from 8 to 40 neurons were considered for the mapping and the de-mapping layers and from 2 to 6 neurons for the bottleneck layer. After trials and errors, the structure of 8:15:3:15:8 was selected for the AANN. By using the training samples generated with the engine model, typically around 559 iterations were required to train the AANN and achieve an MSE value of 0.00118.

Figure 10 shows the visualization of the seven component faults considered in this paper using 3 PCs. The axes represent the PCs and each colored group represents the features of the sample data corresponding to

each fault class. The patterns spreading radially outward indicate faulty engine conditions with increasing severity levels. The furthest points are associated with maximum severities, whereas the closest points correspond to low-level faults. We can see that the data are not linearly separable. This implies that nonlinear classifiers may be more suitable than the linear ones. Besides, it was observed that as the noise level increases the overlapping possibilities of the adjacent classes increase. This may increase the difficulty of obtaining clear decision boundaries between neighbor classes. Thus, an AANN based dimension reduction can be used for an effective visualization of engine faults and understand their nature even in a high-noise environment.

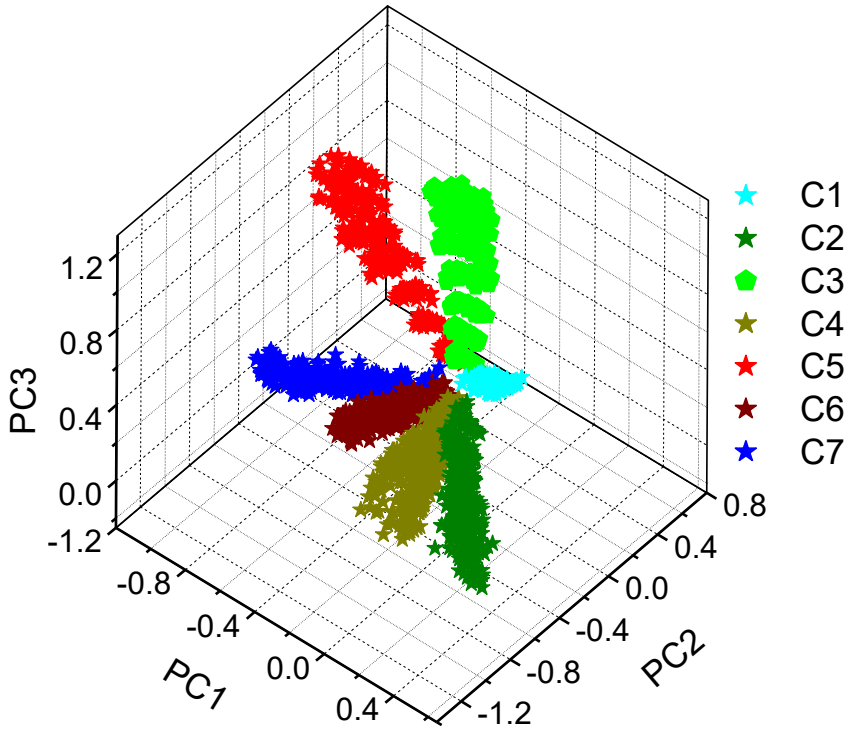

Fig. 10. AANN based gas path component fault visualization using 3 PCs

4.2 Fault Detection and Isolation

The detection and isolation performance of the proposed method were evaluated using 4743 samples. Table 4 demonstrates the training and test samples used and the classification success rates achieved. The classification success rates were computed from the obtained confusion metric based on Eqs. (24-31) (49).

$$\text{True positive rate (TPR)} = \frac{\text{Number of correct fault detections}}{\text{Number of fault cases}} = \frac{\text{NCFD}}{\text{NFC}} \tag{24}$$

$$\text{False negative rate (FNR)} = \frac{\text{Number of incorrect NF detections}}{\text{Number of fault cases}} = \frac{\text{NINFD}}{\text{NFC}} \tag{25}$$

$$\text{False positive rate (FPR)} = \frac{\text{Number of incorrect fault detections}}{\text{Number of NF cases}} = \frac{\text{NIFD}}{\text{NNFC}} \tag{26}$$

$$\text{True negative rate (TNR)} = \frac{\text{Number of correct NF detections}}{\text{Number of NF cases}} = \frac{\text{NCNFD}}{\text{NNFC}} \tag{27}$$

$$\text{Overall detection accuracy (ODA)} = \frac{\text{NCFD} + \text{NCNFD}}{\text{NFC} + \text{NNFC}} \tag{28}$$

$$\text{Correct classification rate (CCR)} = \frac{\text{Number of correct classifications}}{\text{Number of cases of the fault}} = \frac{\text{NCC}}{\text{NCF}} \tag{29}$$

$$\text{Incorrect fault classification rate (IFCR)} = \frac{\text{Number of misclassifications}}{\text{Number of cases of the fault}} = \frac{\text{NMC}}{\text{NCF}} \tag{30}$$

$$\text{Overall classification accuracy (OCA)} = \frac{\text{Total number of correct classifications}}{\text{Total number of cases of the faults}} \tag{31}$$

The classification accuracy of SVM1 represents the detection accuracy of the system. On average, 98% of the test samples were correctly classified. As far as SVM2 is concerned, SCF and MCF categories were classified with a success rate of 94.5%. Similarly 99.51% of the samples belonging to DCF and TCF groups were classified correctly. The misclassifications were observed when the effects of fault severity levels of

SCFs and DCFs or DCFs and TCFs are equivalent. Likewise, Each SCF was classified successfully with a 100% accuracy while an average classification accuracy of 99.98% was achieved from DCF classifications.

Table 4: Classification accuracy of the SVM based classifiers

Classifier	Used to classify	No. of input samples	No. of correctly classified samples	OCA (%)
SVM1	F/NF	4743	4609	98.5
SVM2	SCF/MCF	4284	4090	94.5
SVM3	C1/(C2+C3)	1836	1836	100
SVM4	C2/(C1+C3)	1836	1836	100
SVM5	C3/(C1+C2)	1836	1836	100
SVM6	DCF/TCF	2448	2436	99.51
SVM7	C4/(C5+C6)	1836	1836	100
SVM8	C5/(C4+C6)	1836	1836	100
SVM9	C6/(C4+C5)	1836	1833	99.94

4.2.1 Effect of Number of Measurements

It is understandable that a diagnostic algorithm requiring few numbers of sensors and delivering accurate diagnostic predictions is preferable. However, lack of sufficient information may affect faults' distinguishability, particularly when two or more simultaneous faults are considered. This portion of the experimentation was assigned to assess the fault classification capability of our proposed method using three randomly selected sets of measurements and compare with the results obtained from 8 sensors.

- Set 1: P3, T3, $N_{GG,}$ $W_{f,}$ and T4

- Set 2: P3, T3, $N_{GG,}$ $W_{f,}$, P4, and T4
- Set 3: P3, T3, $N_{GG,}$ $W_{f,}$, P4, T4, and T5

Table 5 presents the classification results obtained. Generally, the accuracies achieved in all the cases were good enough to make a fault classification decision although about 2.3% performance loss was observed between the 5 and 8 sensors. This may indicate the capability of SVMs for gas path component fault detection and isolation with limited information. As expected, SVM1, SVM2, and SVM6 provided lesser success rates than the other SVM classifier models due to the number and type of faults taken into account (as illustrated in Table 1). A similar observation to the cases of SVM2 and SVM6 was also reported so far for ANNs (41).

Table 5: Classification performance of SVM classifiers using different numbers of measurements

Classifier	Classification accuracy (%)			
	5 sensors	6 sensors	7 sensors	8 sensors
SVM1	97.5	97.8	98.0	98.5
SVM2	90.1	92.7	93.9	94.5
SVM3	99.6	99.8	99.8	100
SVM4	99.5	99.6	99.8	100
SVM5	99.4	99.6	99.9	100
SVM6	91.5	92.5	95.1	99.51
SVM7	99.4	99.8	100	100
SVM8	99.3	100	100	100
SVM9	99.2	99.82	99.84	99.94

4.2.2 Comparison of SVM vs. MLP

In order to evaluate the advantage of the hybrid method over the general single-ANN-based technique, the classification part of the hybrid framework is changed by nested MLP modules. For each component fault scenario, an individual MLP model is used. The classification is then performed based on a binary decision logic, i.e., the input patterns are considered as a signal which is 1 for fault pattern that the network trained to identify, and 0 otherwise. The percentage accuracy obtained from both SVM and MLP modules is given in Table 6. From this table, it can be seen that the SVM provided better classification accuracy in all the fault scenarios than the MLP method, especially with high-level measurement noise. The degree of influence of measurement noise on the classification effectiveness of an MLP is also investigated in (36). In general, on average, the classification performance of the hybrid method showed over 12 % improvement than the general MLP based scheme. Without the noise filtering algorithm, the classification accuracy depreciates from the average 87% to 78% at the maximum noise level of ± 2σ.

Table 6 Gas turbine gas path fault classification performance of SVM vs MLP

Fault type	Classification Accuracy (%)	
	SVM (combined with AANN)	MLP (without AANN)
CF	100	88.3
GGTE	100	87.8
PTE	100	87.9
CF+GGTE	99.51	87.1
CF+PTE	100	87.3
GGTE+PTE	100	87.4

CF+GGTE+PTE	99.94	86.1

4.3 Fault Identification

The fault identification model was trained by using the training samples derived from the seven component fault scenarios. In the hidden layer of the network, 5 to 50 neurons were considered. Different configurations for the MLP neural network were evaluated by trials and errors and finally the configuration of 8:35:6 was selected. Typically around 1000 iterations were required for the training to achieve an MSE value closer to 0.0003. Randomly selected test samples were then used for testing and the results are given in Table 7. An important observation from this table is that for each of the approximation model, in all the cases, the mean of the estimation errors approaches to zero.

Figure 11 shows the estimation error distribution of the fault identification network on the 1176 test samples. The decision whether the estimation results of flow capacity and efficiency parameters are good enough to suggest this technique for practical use or not should be made based on the confidence interval they provide. With reference to the confidence level of the fault estimation, as presented in Figure 12, about 80% of the samples estimation error lied within $\pm 1\sigma$; over 95.2% within $\pm 2\sigma$; and over 99% within $\pm 3\sigma$ of the mean. On the other hand, according to Eq. (22), say for example, for a given compressor deterioration value of -3% decrease in flow capacity and -1% decrease in isentropic efficiency due to fouling, the fault estimation network is over 95% confident to provide prediction values within the range of -3 ± 0.0185 and -1 ± 0.0383, respectively. This prediction accuracy is adequately sufficient to make a maintenance decision. Similarly, as shown in Table 7, ρ values for all performance parameters are very close to 1. This indicates a

very strong correlation between the predicted and target fault values. Moreover, the flow capacity ρ values were a bit higher than that of the isentropic efficiency. This kind of correlation difference between these parameters is often expected due to their associated fault levels considered (41). Table 8 demonstrates the fault estimation results for some randomly selected fault cases. As shown in this table, the estimation accuracies are generally very good. Out of the 12 test cases considered, the maximum error is about 7% in a TCF scenario and the contribution of the individual prediction outliers to the overall accuracy was insignificant. Increasing the training and test samples reduces their corresponding MSE values. Moreover, the accuracy may also be improve using individual networks for each fault case.

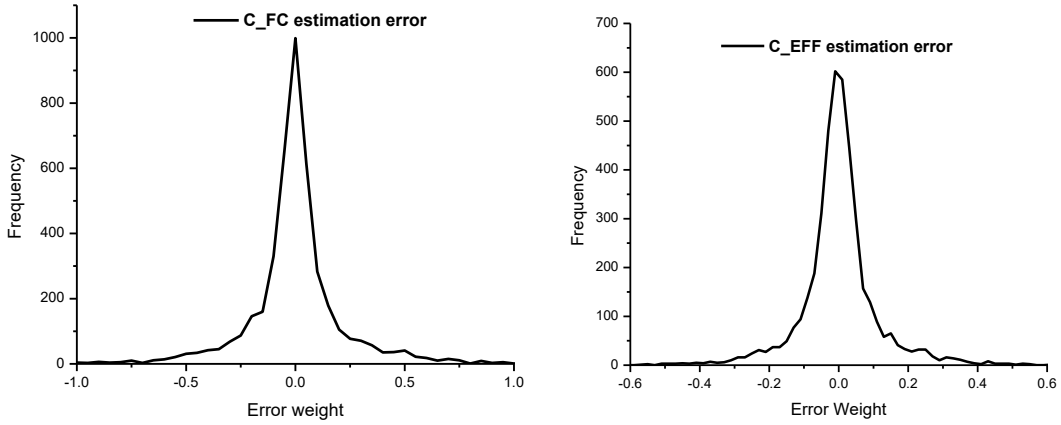

(a) (b)

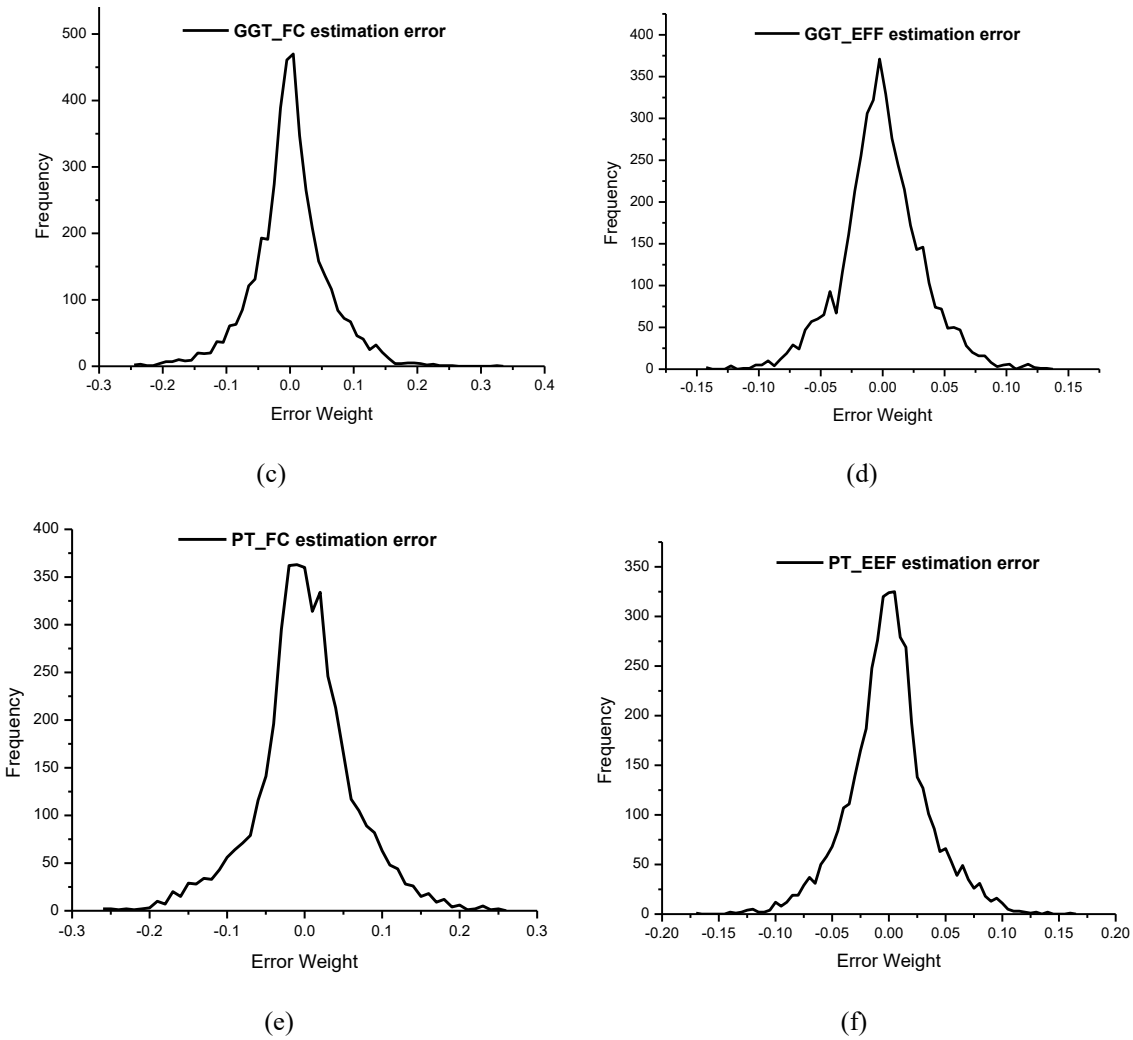

Fig. 11. (a-f) Actual estimation error distribution of each health parameter

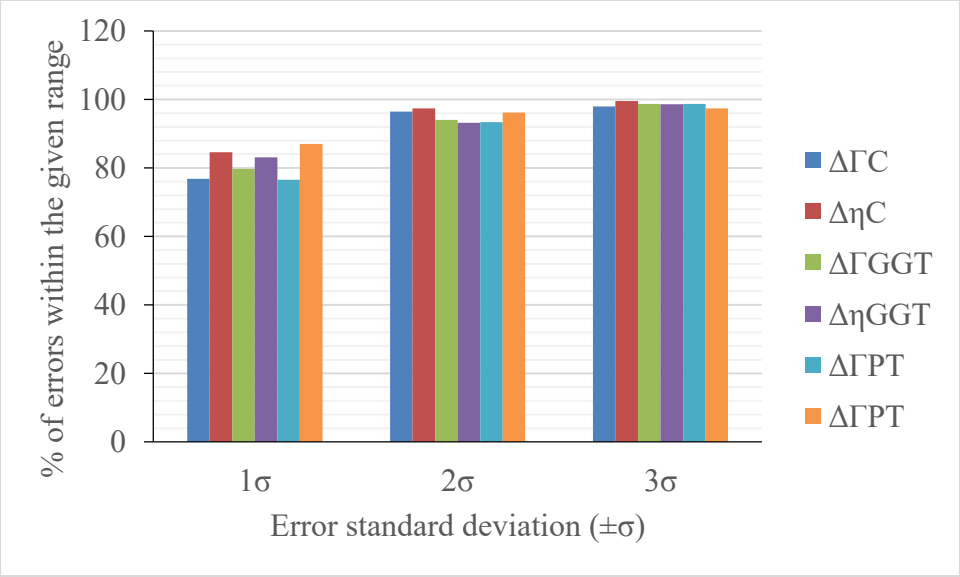

Fig. 12. Confidence level of the fault estimation

Table 7: Mean, standard deviation and correlation coefficient values of the fault estimation

	$\Delta\Gamma_C$	$\Delta\eta_C$	$\Delta\Gamma_{GGT}$	$\Delta\eta_{GGT}$	$\Delta\Gamma_{PT}$	$\Delta\eta_{PT}$
μ	-0.011	-0.005	-0.004	0.002	-0.003	0.001
σ	0.264	0.134	0.066	0.033	0.067	0.035
ρ	0. 9920	0.9768	0.9987	0.9895	0.9981	0.9811

Table 8: Sample test results of randomly selected fault cases

Fault	Implanted fault (%)						Predicted fault (%)					
	CF		GGTE		PTE		CF		GGTE		PTE	
	ΔΓ	Δη	ΔΓ	Δη	ΔΓ	Δη	ΔΓ	Δη	ΔΓ	Δη	ΔΓ	Δη
C1	-1.5	-1.2	0	0	0	0	-1.54	-1.220	0.004	-0.004	0.012	-0.011
	-4	-3.2	0	0	0	0	-3.95	-3.160	0.001	-0.001	0.000	0.000

C2	0	0	1.5	-1.2	0	0	-0.002	-0.003	1.508	-1.205	0.000	0.000
	0	0	4	-3.2	0	0	-0.002	-0.003	4.016	-3.208	0.000	0.000
C3	0	0	0	0	1.5	-1.2	-0.001	-0.002	0.003	-0.003	1.515	-1.201
	0	0	0	0	4	-3.2	0.000	0.000	0.001	-0.001	3.98	-3.194
C4	-1.5	-1.2	1.5	-1.2	0	0	-1.478	-1.186	1.486	-1.194	0.000	0.000
	-4	-3.2	4	-3.2	0	0	-3.910	-3.148	3.966	-3.187	0.000	0.000
C5	-1.5	-1.2	0	0	1.5	-1.2	-1.477	-1.193	0.002	-0.002	1.512	-1.210
	-4	-3.2	0	0	4	-3.2	-3.962	-3.178	0.001	-0.001	4.045	-3.227
C6	0	0	1.5	-1.2	1.5	-1.2	-0.001	-0.003	1.492	-1.173	1.501	-1.191
	0	0	4	-3.2	4	-3.2	-0.001	-0.002	4.003	-3.195	3.998	-3.164
C7	-1.5	-1.2	1.5	-1.2	1.5	-1.2	-1.518	-1.228	1.518	-1.211	1.477	-1.185
	-4	-3.2	4	-3.2	4	-3.2	-3.910	-3.152	4.022	-3.205	4.017	-3.211

CONCLUSIONS

A hybrid ANN and SVM method for a two-shaft industrial GT engine gas path diagnosis has been presented. It consists of hierarchically arranged several modules trained to handle specific activities. The first module uses an AANN to minimize noise and extract important Principle Component features and integrated with nested SVM classifiers where abnormal operating conditions are detected and isolated, followed by an MLP approximator where the magnitudes of the faults are estimated. The test results showed that the proposed method, in general, is capable of diagnosing major gas path component faults with high accuracies. Moreover, the level of accuracy obtained confirms that combined methods have derivable advantages over the individual methods, particularly over those designed to perform single and multiple component faults together. Specifically, 3/3 SCF and 2/3 DCF classes have been classified successfully with a 100% accuracy, while a 5.5% of the TCFs were misclassified. In regard to the fault

identification performance, the MLP network is over 95% confident to yield predictions within the maximum range of actual value ± 0.0766 for flow capacity and actual value ± 0.0383 for isentropic efficiency. Finally, the effect of the number of sensors on the diagnostic accuracy has been studied. The comparative result indicated that the fault classification part of the system provided 96.8% average accuracy with 5 sensors, which is about 2.3% lower than the result owned by 8 sensors. Eventually, the proposed method can be implemented as a gas path diagnostic system for a two-shaft GT engine under steady-state operating conditions, even with a limited number of gas path measurements.

ACKNOWLEDGMENT

The authors would like to acknowledge Universiti Teknologi PETRONAS (UTP) for supporting this research financially (YUTP project cost center no. 0153AA-A84).

REFERENCES

1. Tahan M, Tsoutsanis E, Muhammad M, Karim ZA. Performance-based health monitoring, diagnostics and prognostics for condition-based maintenance of gas turbines: A review. Applied Energy. 2017;198:122-44.

2. Ogaji SOT-o. Advanced Gas-path Fault Diagnostics for Stationary Gas Turbines [Ph.D. Thesis]: Cranfield University, UK; 2003.

3. Singh R. Advances and opportunities in gas path diagnostics. 15th ISABE, Paper No ISABE-2003-1008. 2003.

4. Marinai L, Probert D, Singh R. Prospects for aero gas-turbine diagnostics: A review. Applied Energy. 2004;79(1):109-26.

5. Zedda M, Singh R. Neural-network-based sensor validation for gas turbine test bed analysis. Proceedings of the Institution of Mechanical Engineers Part I: Journal of Systems and Control Engineering. 2001;215(1):47-56.

6. Ogaji SOT, Singh R, Probert SD. Multiple-sensor fault-diagnoses for a 2-shaft stationary gas-turbine. Applied Energy. 2002;71(4):321-39.

7. Joly RB, Ogaji SOT, Singh R, Probert SD. Gas-turbine diagnostics using artificial neural-networks for a high bypass ratio military turbofan engine. Applied Energy. 2004;78(4):397-418.

8. Xiradakis N, Li YG, editors. Gas turbine and sensor fault diagnosis with nested artificial neural networks. Proceedings of the ASME Turbo Expo 2004; 2004.

9. Ogaji SOT, Li YG, Sampath S, Singh R. Gas Path Fault Diagnosis of a Turbofan Engine From Transient Data Using Artificial Neural Networks. 2003(36843):405-14.

10. Sina Tayarani-Bathaie S, Khorasani K. Fault detection and isolation of gas turbine engines using a bank of neural networks. Journal of Process Control. 2015;36:22-41.

11. Sadough Vanini ZN, Meskin N, Khorasani K. Multiple-Model Sensor and Components Fault Diagnosis in Gas Turbine Engines Using Autoassociative Neural Networks. Journal of Engineering for Gas Turbines and Power. 2014;136(9):091603-.

12. Courdier A, Li YG. Power Setting Sensor Fault Detection and Accommodation for Gas Turbine Engines Using Artificial Neural Networks. 2016(49828):V006T05A5.

13. Amozegar M, Khorasani K. An ensemble of dynamic neural network identifiers for fault detection and isolation of gas turbine engines. Neural Networks. 2016;76:106-21.

14. Xia F, Zhang H, Peng D, Li H, Su Y. Turbine Fault Diagnosis Based on Fuzzy Theory and SVM. Artificial Intelligence and Computational Intelligence. 2009:668-76.

15. Zhou D, Zhang H, Weng S. A new gas path fault diagnostic method of gas turbine based on support vector machine. Journal of Engineering for Gas Turbines and Power. 2015;137(10):102605.
16. Widodo A, Yang B-S. Support vector machine in machine condition monitoring and fault diagnosis. Mechanical systems and signal processing. 2007;21(6):2560-74.
17. Meyer D, Leisch F, Hornik K. The support vector machine under test. Neurocomputing. 2003;55(1):169-86.
18. Kramer MA. Neutral network applications in chemical engineeringAutoassociative neural networks. Computers & Chemical Engineering. 1992;16(4):313-28.
19. Zedda M. Gas turbine engine and sensor fault diagnosis: Cranfield University; 1999.
20. Sampath S. Fault diagnostics for advanced cycle marine gas turbine using genetic algorithm: Cranfield University; 2003.
21. Ganguli R. Gas Turbine Diagnostics: Signal Processing and Fault Isolation: CRC press; 2012.
22. Lu PJ, Hsu TC. Application of autoassociative neural network on gas-path sensor data validation. Journal of Propulsion and Power. 2002;18(4):879-88.
23. Lu P, Zhang M, Hsu T, Zhang J. An evaluation of engine faults diagnostics using artificial neural networks. Journal of Engineering for Gas Turbines and Power(Transactions of the ASME). 2001;123(2):340-6.
24. Wang Z, Zhao N, Wang W, Tang R, Li S. A fault diagnosis approach for gas turbine exhaust gas temperature based on fuzzy C-means clustering and support vector machine. Mathematical Problems in Engineering. 2015;2015.

25. Yu W, Liu T, Valdez R, Gwinn M, Khoury MJ. Application of support vector machine modeling for prediction of common diseases: the case of diabetes and pre-diabetes. BMC medical informatics and decision making. 2010;10(1):16.

26. Parikh KS, Shah TP. Support Vector Machine – A Large Margin Classifier to Diagnose Skin Illnesses. Procedia Technology. 2016;23:369-75.

27. Brown MP, Grundy WN, Lin D, Cristianini N, Sugnet CW, Furey TS, et al. Knowledge-based analysis of microarray gene expression data by using support vector machines. Proceedings of the National Academy of Sciences. 2000;97(1):262-7.

28. Burbidge R, Trotter M, Buxton B, Holden S. Drug design by machine learning: support vector machines for pharmaceutical data analysis. Computers & chemistry. 2001;26(1):5-14.

29. Cai Y-d, Lin SL. Support vector machines for predicting rRNA-, RNA-, and DNA-binding proteins from amino acid sequence. Biochimica et Biophysica Acta (BBA)-Proteins and Proteomics. 2003;1648(1-2):127-33.

30. Hua S, Sun Z. A novel method of protein secondary structure prediction with high segment overlap measure: support vector machine approach1. Journal of molecular biology. 2001;308(2):397-407.

31. Sun Y-F, Fan X-D, Li Y-D. Identifying splicing sites in eukaryotic RNA: support vector machine approach. Computers in biology and medicine. 2003;33(1):17-29.

32. Ray P, Mishra DP. Support vector machine based fault classification and location of a long transmission line. Engineering science and technology, an international journal. 2016;19(3):1368-80.

33. Biswas SK, Mia MMA. Image Reconstruction Using Multi Layer Perceptron (MLP) And Support Vector Machine (SVM) Classifier And Study Of Classification Accuracy. International Journal of Scientific & Technology Research. 2015;4(2):226-31.

34. Fahmi BR, Kaouther N, Trabelsi A. Support vector machines versus multi-layer perceptrons for reducing false alarms in intensive care units. International Journal of Computer Applications. 2012;49(11).
35. Zanaty E. Support vector machines (SVMs) versus multilayer perception (MLP) in data classification. Egyptian Informatics Journal. 2012;13(3):177-83.
36. Matuck GR, Barbosa JoR, Bringhenti C, Lima I. Multiple Faults Detection of Gas Turbine by MLP Neural Network. 2009(48821):697-703.
37. Kumar R, Jayaraman VK, Kulkarni BD. An SVM classifier incorporating simultaneous noise reduction and feature selection: illustrative case examples. Pattern Recognition. 2005;38(1):41-9.
38. Cherkassky V, Mulier FM. Learning from data: concepts, theory, and methods: John Wiley & Sons; 2007.
39. Hornik K, Stinchcombe M, White H. Multilayer feedforward networks are universal approximators. Neural Networks. 1989;2(5):359-66.
40. Provost M, Singh R. Gas-path analysis: preparing for success. ROLLS ROYCE PLC-REPORT-PNR. 1995.
41. Ogaji SO, Singh R. Advanced engine diagnostics using artificial neural networks. Applied Soft Computing. 2003;3(3):259-71.
42. Visser WPJ. Generic Analysis Methods for Gas Turbine Engine Performance: The development of the gas turbine simulation program GSP. 2015.
43. Aker GF, Saravanamuttoo HIH. Predicting gas turbine performance degradation due to compressor fouling using computer simulation techniques. Journal of Engineering for Gas Turbines and Power. 1989;111(2):343-50.

44. Mohammadi E, Montazeri-Gh M. Simulation of Full and Part-Load Performance Deterioration of Industrial Two-Shaft Gas Turbine. Journal of Engineering for Gas Turbines and Power. 2014;136(9):092602.
45. Saravanamuttoo H, Lakshminarasimha A. A preliminary assessment of compressor fouling. ASME paper. 1985(85-GT):153.
46. Zwebek A, Pilidis P. Degradation effects on combined cycle power plant performance - Part I: Gas turbine cycle component degradation effects. Journal of Engineering for Gas Turbines and Power. 2003;125(3):651-7.
47. Mohammadi E, Montazeri-Gh M. A fuzzy-based gas turbine fault detection and identification system for full and part-load performance deterioration. Aerospace Science and Technology. 2015;46:82-93.
48. Li Y. Gas turbine performance and health status estimation using adaptive gas path analysis. Journal of Engineering for Gas Turbines and Power. 2010;132(4):041701.
49. Simon DL. Propulsion Diagnostic Method Evaluation Strategy (ProDiMES) User's Guide. 2010.

2018-11-18

Performance-based fault diagnosis of a gas turbine engine using an integrated support vector machine and artificial neural network method

Fentaye, Amare

SAGE

Fentaye AD, Ul-Haq Gilani SI, Baheta AT, Li YG. (2019) Performance-based fault diagnosis of a gas turbine engine using an integrated support vector machine and artificial neural network method. Proceedings of the Institution of Mechanical Engineers, Part A: Journal of Power and Energy, Volume 233, Issue 6, September 2019, pp. 786-802

https://doi.org/10.1177/0957650918812510